PHYSICAL REVIEW B **96**, 201104(R) (2017)

Fate of interaction-driven topological insulators under disorder

Jing Wang,[1,2,3] Carmine Ortix,[2,4] Jeroen van den Brink,[2,5] and Dmitry V. Efremov[2]

[1]*Department of Modern Physics, University of Science and Technology of China, Hefei, Anhui 230026, People's Republic of China*

[2]*Institute for Theoretical Solid State Physics, IFW Dresden, Helmholtzstraße 20, 01069 Dresden, Germany*

[3]*Department of Physics, Tianjin University, Tianjian 300072, People's Republic of China*

[4]*Institute for Theoretical Physics, Center for Extreme Matter and Emergent Phenomena, Utrecht University, Princetonplein 5, 3584 CC Utrecht, The Netherlands*

[5]*Institute for Theoretical Physics, TU Dresden, 01069 Dresden, Germany*

(Received 19 November 2016; revised manuscript received 29 April 2017; published 8 November 2017)

We analyze the effect of disorder on the weak-coupling instabilities of a quadratic band crossing point (QBCP) in two-dimensional Fermi systems, which, in the clean limit, display interaction-driven topological insulating phases. In the framework of a renormalization group procedure, which treats fermionic interactions and disorder on the same footing, we test all possible instabilities and identify the corresponding ordered phases in the presence of disorder for both single-valley and two-valley QBCP systems. We find that disorder generally suppresses the critical temperature at which the interaction-driven topologically nontrivial order sets in. Strong disorder can also drive a topological phase transition into a topologically trivial insulating state.

DOI: 10.1103/PhysRevB.96.201104

The study of topological phases of matter is one of the most active research areas in contemporary condensed-matter physics. The explanation of the quantum Hall effect in terms of the topological properties of the Landau levels [1,2] in the 1980s triggered an intense research effort in the theoretical prediction [3–5] and the experimental discovery [6,7] of a plethora of different topologically nontrivial quantum phases. In two-dimensional (2D) insulating systems only two distinct topological nontrivial phases can be realized according to the well-established classification of topological insulators and superconductors [8,9]: (i) the quantum anomalous Hall (QAH) state [3] with a time-reversal symmetry-broken ground state and topologically protected chiral edge states and (ii) the time-reversal invariant quantum spin Hall (QSH) state [4,5], which possesses helical edge states with counterpropagating electrons of opposite spins.

In recent years, attention has gradually shifted from noninteracting topological states of matter toward *interaction-driven topological phases*: many-particle quantum ground states in which chiral orbital currents or spin-orbit couplings are spontaneously generated by electronic correlations. These states of matter possess both conventional order, characterized by an order parameter and a broken symmetry, and protected edge states associated with a topological quantum number. Interaction-driven QAH and QSH phases were first conceived in the context of 2D honeycomb lattice Dirac fermions [10] assuming sufficiently strong electronic repulsions, although more recent analytical and numerical works question the proposal for this particular model [11–14].

On the contrary, it has been proposed that 2D systems with a quadratic band crossing point (QBCP) are unstable to electronic correlation because of the finite density of states at the Fermi level leading to the possibility of weak-coupling interaction-driven topological insulating phases [15–18]. And, indeed, QAH and QSH phases generated by electronic repulsions occur both in the checkerboard lattice model [15,19], and in two-valley QBCP models for bilayer graphene [20,21]. A question that naturally arises is whether and how these weak-coupling interaction-driven states are affected by the presence of disorder, which is well known to induce prominent phenomena such as Anderson localization, metal-insulator transition, and phase transitions between superconducting phases [22–28]. For 2D topological states of matter this question is of particular importance, as the global topological nature of the ground state should render such states, in principle, robust against the local effects of disorder [29].

In this work, we analyze the fate of the interaction-driven topological insulators in Fermi systems with a QBCP under the effect of three different types of disorders, which preserve time-reversal symmetry [24]. Depending on their couplings with fermions, we refer to these as random chemical potential, random mass, and random gauge potential [30]. These different sorts of disorders have been shown to give rise to distinct behaviors of fermionic systems [31–44]. In general, the effect of disorder is essential in 2D for itinerant systems since it may lead to localization. Therefore interactions and disorder must be treated on equal footing and we subsequently go beyond a mean-field analysis of disorder and employ the perturbative renormalization group (RG) technique [45–47]. The renormalization flow procedure starts at high energy, when the ground state is known, and ends with a leading instability, which is characterized by a corresponding fixed point (FP). The analysis of the interplay of the phases well below T_c is out of scope of this Rapid Communication. The central result of our calculations is schematically illustrated in Fig. 1 for the random chemical potential. With disorder the fixed points evolve to new positions, which correspond to topological phase transitions to trivial insulating states in the strong disorder regime. Moreover, the analysis of the evolution of the FP shows that disorder generally suppresses the critical temperature at which the interaction-induced topological insulating states set in.

Checkerboard lattice. The low-energy theory of spin one-half fermions on a checkerboard lattice in the presence of disorder is described by the Hamiltonian $H = H_0 + H_{\rm int} + H_{\rm dis}$,

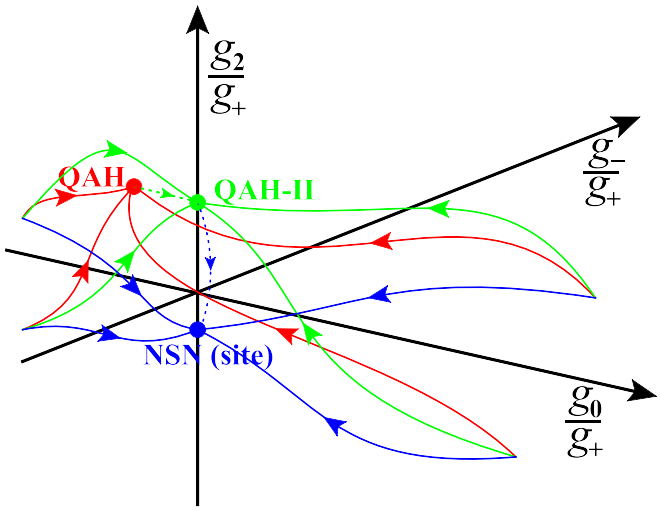

FIG. 1. Schematic renormalization group flows of the coupling constant ratios $(g_0^*,g_-^*,g_2^*)/g_+^*$ for the checkerboard lattice in the clean limit (red) and in the presence of random chemical potential (green and blue). In clean limit the QAH fixed point $(g_0^*,g_-^*,g_2^*)/g_+^* = (0,-3.73,7.46)$ (red point) corresponds to a QAH state. In the presence of the weak random chemical potential the coupling constants flow to the QAH-II fixed point (green) $(g_0^*,g_-^*,g_2^*)/g_+^* = (0,-0.2,6.5)$ corresponding again to the QAH state and in the presence of the strong random chemical potential to the NSN fixed point (green) $(g_0^*,g_-^*,g_2^*)/g_+^* = (0,0,-1.09)$ corresponding to the NSN (site) state. The dashed lines represent all virtual trajectories to change the fixed points with impurities. The relationship between fixed points QAH and QAH-II is provided in the inset figure of Fig. 2(a).

where H_0 is the kinetic energy, which is invariant under the C_{4v} point group and time-reversal symmetry [15]. It reads

$$H_0 = \sum_{|\mathbf{k}|<\Lambda}\sum_{\sigma=\uparrow\downarrow} \psi^\dagger_{\mathbf{k}\sigma}\mathcal{H}_0(\mathbf{k})\psi_{\mathbf{k}\sigma}, \tag{1}$$

$$\mathcal{H}_0(\mathbf{k}) = t_I\mathbf{k}^2\tau_0 + 2t_x k_x k_y\tau_1 + t_z\left(k_x^2 - k_y^2\right)\tau_3, \tag{2}$$

where Λ is the momentum cutoff, while $\psi_{\mathbf{k}\sigma}$ has two components corresponding to the two sublattices of the checkerboard lattice and τ_i are Pauli matrices. Without loss of generality, we will consider in the remainder the parameter set $t_I = 0$ and $t_x = t_z = t$, which corresponds to a particle-hole symmetric QBCP [15,19,48] and the parameter t is rescaled by $1/2m$ (here and below we assume $\hbar = 1$). The interacting part of the Hamiltonian $H_{\rm int}$ has the general form [15,19,48–50]

$$H_{\rm int} = \frac{2\pi}{m}\sum_{i=0}^{3} g_i \int d^2\mathbf{x}\left(\sum_{\sigma=\uparrow\downarrow}\psi^\dagger_\sigma(\mathbf{x})\tau_i\psi_\sigma(\mathbf{x})\right)^2. \tag{3}$$

As mentioned above, we will consider three types of disorder: (1) random chemical potential, (2) random gauge potential, and (3) random mass. Its general representation adopted from Refs. [24,30,44] is

$$H_{\rm dis} = \nu_m \int d^2\mathbf{x}\,\psi^\dagger(\mathbf{x})M\psi(\mathbf{x})A(\mathbf{x}). \tag{4}$$

Here $M = \tau_0$ is the random chemical potential, $M = \tau_1$ and $M = \tau_3$ the random gauge potential (two components), and $M = \tau_2$ the random mass disorders. The field $A(\mathbf{x})$ represents a quenched, Gauss-white potential determined by $\langle A(\mathbf{x})\rangle = 0$, while $\langle A(\mathbf{x})A(\mathbf{x}')\rangle = n_0\delta(\mathbf{x}-\mathbf{x}')$, where n_0 is the impurity (defects) concentration. The impurity scattering rate we quantify by $\tau^{-1} = n_0\nu_m^2/t$, which will be measured by $\Lambda_E = t\Lambda^2$ [for more details, see Supplemental Material (SM) [51]]. In general, a complete analysis should contain all possible fermion bilinears including those appearing due to interaction effects. However, we focus here on the suppression of the topological phases by disorder. Therefore for the sake of simplicity we restrict ourself to the effect of the aforementioned types of disorder separately.

RG analysis and fixed points. Within the Wilsonian renormalization group theory [20,45–47,52–56], we derive the flow equations by integrating out the fields in the momentum shell $e^{-l}\Lambda < k < \Lambda$, with $l > 0$ the running scale, integrating over all frequencies at the same time. The disorder contributes both to the fermion self-energy renormalization and to vertices renormalization. As a result, we obtain a system of flow equations for the coupling constants g_i and disorder potentials ν_m and t in the form [15,19,48]

$$\frac{dg_i}{dl} = \sum_{jk} A_{ijk}g_j g_k + \sum_j B_{ij}\frac{n_0\nu_m^2}{\pi t^2}g_j,$$

$$\frac{d\nu_m}{dl} = \left(D_0\nu_m + t\sum_i D_i g_i\right)\frac{n_0\nu_m^2}{\pi t^2},$$

$$\frac{dt}{dl} = -C\frac{n_0\nu_m^2}{\pi t^2}t, \tag{5}$$

where the coefficients A_{ijk}, B_{ij}, C, D_0, and D_i are provided in the SM [51]. The FPs are subsequently determined from the numerical analysis of the flow equations (5). Solving the flow equations in the clean limit [19,48] leads to three fixed points $(g_0^*,g_-^*,g_2^*) = (0,-3.73,7.46)g_+$, $(g_0^*,g_-^*,g_2^*) = (0,3.73,7.46)g_+$, and $(g_0^*,g_-^*,g_2^*) = (0,0,-1.09)g_+$, where $g_\pm = (g_3 \pm g_1)/2$. The first two fixed points correspond to the QAH order, while the last one corresponds to QSH.

Under the influence of the disorder the fixed points move in the space of the coupling constants. The evolution of the FP $(0,-3.73,7.46)g_+$ and FP $(g_0^*,g_-^*,g_2^*) = (0,0,-1.09)g_+$ with increasing the strength of the bare random chemical potential are shown in the inset figures of Fig. 2. They gradually change with the increase of the bare values of disorder and saturate with an intermediate plateau, designated as QAH (QSH) and QAH-II (QSH-II,III) FPs in Fig. 2 (here and below for easy identification we label the fixed points by the corresponding ground states QAH and QSH). We found that other evolutions are also possible (for disorders of the random mass and random gauge potential types see [51]).

Susceptibilities and phase diagrams. To find the phases that are realized at the FPs, we next solve the flow equations for the order parameters Δ_i corresponding to the different long-range orders allowed by the symmetries of the corresponding crystal structures. All possible order parameters for the checkerboard and honeycomb lattices are listed in the SM [51]. In particular, a finite expectation value of the time-reversal symmetry-breaking order parameter $\Delta_{\rm QAH}$ corresponds to a QAH phase with quantized Hall conductivity, as can be shown, in the clean limit and at the mean-field level, by integrating the Berry curvature in the full Brillouin zone (BZ) [15,51]. Similarly,

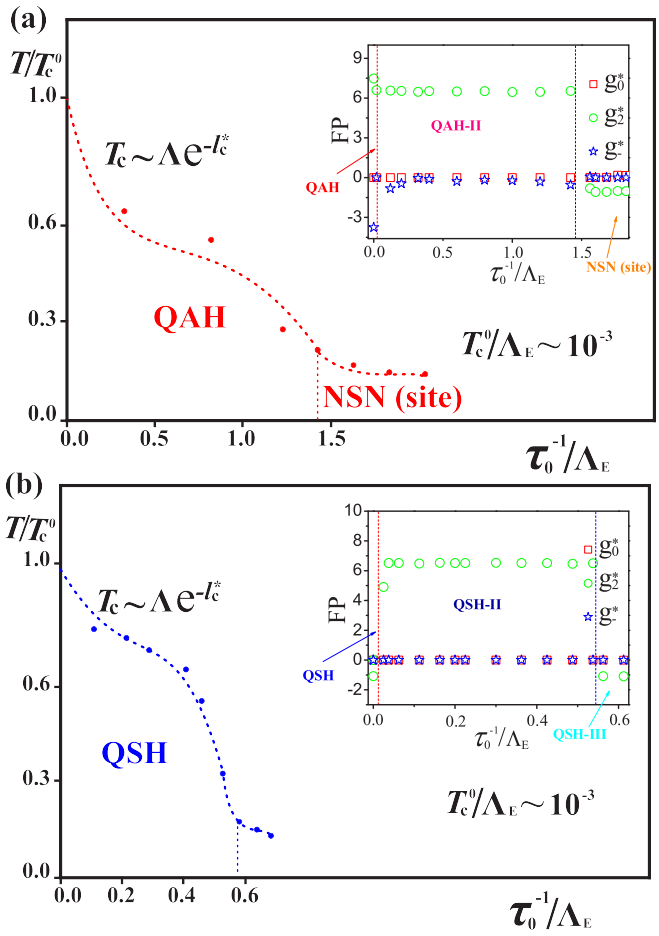

FIG. 2. Schematic phase diagram for the checkerboard lattice in the presence of random chemical potential and which in the clean limit give (a) $(g_0^*, g_-^*, g_2^*) = (0, -3.73, 7.46)g^+$ and (b) $(g_0^*, g_-^*, g_2^*) = (0, 0, -1.09)g^+$. The other two cases are presented in the SM [51]. Insets: Evolution of the (a) QAH fixed points $(g_0^*, g_-^*, g_2^*) = (0, -3.73, 7.46)g_+$ and (b) QSH $(g_0^*, g_-^*, g_2^*) = (0, 0, -1.09)$ with increase of the strength of the bare random mass disorder potential for the checkerboard lattice. The designations QAH and QAH-II (or QSH, QSH-II, and QSH-III) FPs show the regimes, where the FPs are stable with increase of impurity scattering rates. The inset QAH and QSH represent the clean limit case.

the ground state with order parameter Δ_{QSH} signals the onset of the spin-rotation symmetry-breaking QSH phase, which is characterized by the spin Chern number $(C^{\uparrow} - C^{\downarrow})/2$ [57].

Employing the relation $\delta\chi_i(l) = -\frac{\partial^2 \delta f}{\partial \Delta_i(0) \partial \Delta_i^*(0)}$ [19,48,58], where f is the free energy, we can obtain the corresponding susceptibilities approaching the FPs. One finds that near the RG scale l_c^*, where the couplings $g_i(l)$ diverge, $\chi_i(l) \sim (l_c^* - l)^{-\gamma}$. For instance, their behavior as a function of the RG flow around the QAH FP is depicted in Fig. 3 and others are provided in the SM [51]. Therefore the ground state may be obtained as the state characterized by the susceptibility with the strongest divergence or by comparison of the corresponding critical indexes γ_i [19,48]. We checked that both ways give the same results.

Using this procedure we determine the resulting ground state as a function of the ratio of the bare interaction strength

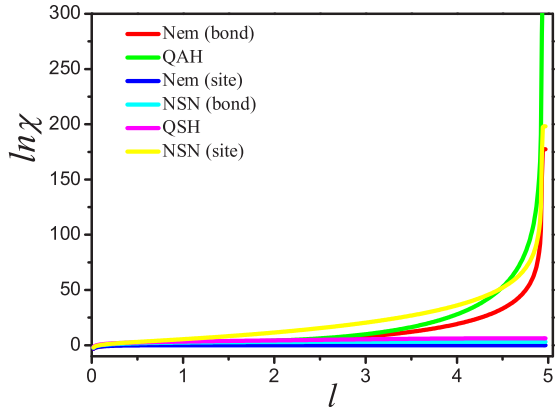

FIG. 3. Susceptibilities to particle-hole phases as functions of the RG flow parameter l by approaching the QAH FP $(g_0^*, g_-^*, g_2^*)/g_+ = (0, -3.73, 7.46)$ for checkerboard lattice.

g_3/g_0 and the disorder strength. The phase diagram for the checkerboard lattice is shown in Fig. 4. Please note that the border lines are drawn schematically and are the matter of further investigations. In the clean limit the $g_3/g_0 < 0.26$ corresponds to the QSH state, while $g_3/g_0 > 0.26$ corresponds to the QAH state [19]. Considering the QAH state in the presence of the chemical potential disorder, one sees that it is changed at certain value of disorder by the spin nematic (NSN) site order. Further increase of disorder potential leads to the nonordered state. In contrast, the QSH state is suppressed by disorder without changes to intermediate phases. For the random mass potential we found no intermediate phases.

To further understand the possible consequences of the fixed-point evolution, we subsequently determine the phase diagram with an effective T dependence, which is linked to the transformation $T = T_0 e^{-l}$ [53,56]. As critical temperature we use the value $T_c = T_0 e^{-l_c^*}$; the results are presented in Fig. 2. Considering the effective critical temperature as a function of the random chemical potential disorder, one notes a considerable change of the T_c slope at the QAH $\rightarrow$ NSN transition in Fig. 2(a). Surprisingly, the slopes also considerably change with evolution of the fixed points within the same phase. This comes from the fast crossovers from one FP to another. An example of such a slope change is provided by the evolution between the QSH-II and QSH-III FPs in Fig. 2(b). The evolution of the FP is gradual and one does not see any characteristic features on T_c [51]. The situation of random mass and random gauge potential is detailed in the SM [51]. Before summarizing the results we have to note that the scattering rate $\tau^{-1}(l)$ is strongly renormalized in 2D together with the interaction [51]. Therefore the experimentally relevant values of the impurity scattering rate are not the bare τ_0 but $\tau^{-1}(l_c^*)$ at the characteristic energy of the instability. The comparison of values of the scattering rate $\tau^{-1}(l_c^*)$ necessary to suppress the effective critical temperature twice with the effective critical temperature T_c^0 in the clean limit is summarized in Table I. As one can see from the table, the critical impurity scattering rates for a complete suppression of the topological phases are of the order of the critical temperature in the clean limit. By considering that the latter corresponds to the dynamically generated gap, we can conclude that, in perfect

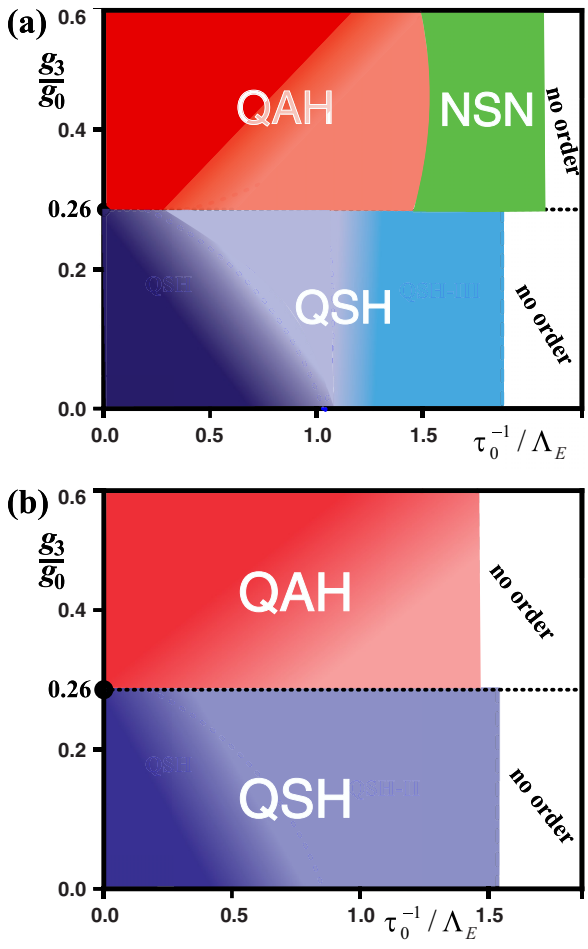

FIG. 4. Schematic phase diagram as a function of disorder and interaction strength g_3/g_0 for the checkerboard lattice. (a) Random chemical potential and (b) random mass. The change of the color from dark to light is deduced from the evolution of the FPs as shown in Fig. 2.

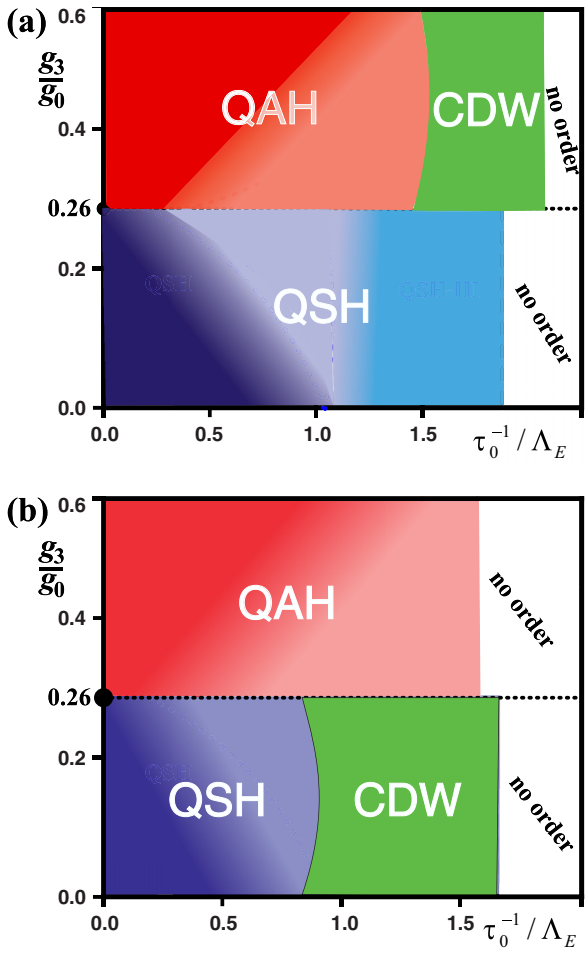

FIG. 5. Schematic phase diagrams for the honeycomb lattice for bare couplings $g_1(l=0)=g_2(l=0)=0$ in the presence of (a) random chemical potential and (b) random mass. The change of the color from dark to light is deduced from the evolution of the FPs as shown in Fig. 2.

analogy with noninteracting topological insulating states [29], the stability of interaction-driven topological insulators is relatively immune to nonmagnetic impurities.

Bilayer graphene. We subsequently generalize our analysis to the honeycomb lattice model for bilayer graphene. At the two inequivalent **K** and **K**′ points of the Brillouin zone, the low-energy bands touch parabolically [16,20,21,59,60] and realize a two-valley QBCP system with an effective Hamiltonian $H = \sum_{\mathbf{k}} \psi^{\dagger}_{\mathbf{k}\sigma} \mathcal{H}_0 \psi_{\mathbf{k}\sigma}$ (the noninteracting Hamiltonian and other information are provided in the SM [51]). The effective action

TABLE I. Stability of the phases against different types of disorder: chemical potential (C), random mass (M), and random gauge potential (G). Here $\tau^{-1}(l^*_{c0})$ is taken at the energy of the first instability in the clean limit.

	QAH	QSH	NSN	CDW
C	$\tau^{-1}(l^*) \sim T_c^0$	$\tau^{-1}(l^*) \sim T_c^0$	$\tau^{-1}(l^*) \gg T_c^0$	$\tau^{-1}(l^*) \gg T_c^0$
M	$\tau^{-1}(l^*) \sim T_c^0$	$\tau^{-1}(l^*) \sim T_c^0$		
G	$\tau^{-1}(l^*) \sim T_c^0$	$\tau^{-1}(l^*) \sim T_c^0$		

[21,48] is similar to that for the checkerboard lattice and provided explicitly in the SM [51]. Despite the effective theory for the checkerboard and the bilayer honeycomb lattice are similar, the latter exhibits many more instabilities [48] due to the additional valley degree of freedom. In order to fully understand the leading instabilities for the bilayer honeycomb lattice, we calculate the susceptibilities for all 18 possible orderings [3,20,21,36,48,61–70]. The resulting disorder phase diagrams for the bilayer honeycomb lattice are shown in Fig. 5. The temperature-dependent phase diagrams at bare $g_1(l=0)=g_2(l=0)=0$ are qualitatively similar to those of the checkerboard lattice, but with the NSN (site) and QSH phases in Fig. 2 replaced by a charge-density-wave (CDW) phase [51].

We have analyzed the fate of the weak-coupling interaction-driven topological insulator phases realized in 2D Fermi systems with a QBCP, under the influence of disorder. By means of the RG approach and unbiasedly studying the fermion-interacting couplings and disorders, we build the coupled flow equations of the fermion-interacting couplings and disorder strength. We established that the different types of

disorder generally suppress the critical temperature at which the interaction-driven topological states set in. In particular cases, strong disorder can even induce phase transition from a topological to a nontopologically ordered state. Disorder in interaction-driven topological systems thus gives rise to a distinct set of phenomena that can be looked for and studied experimentally. Moreover, the response to disorder might be used as an experimental signature that a material is actually in a, so far unobserved, interaction-driven topologically insulating state of matter.

Acknowledgments. We acknowledge J. M. Murray and O. Vafek for useful correspondence and C. Fulga for helpful discussions. J.W. is supported by the National Natural Science Foundation of China under Grant No. 11504360, the China Postdoctoral Science Foundation under Grants No. 2015T80655 and No. 2014M560510, the Fundamental Research Funds for the Central Universities, and the Program of Study Abroad for Young Scholar sponsored by China Scholarship Council. C.O. acknowledges the financial support of the Future and Emerging Technologies Programme for Research of the European Commission under FET-Open Grant No. 618083 (CNTQC), and the Deutsche Forschungsgemeinschaft under Grant No. OR 404/1-1. D.V.E. and J.v.d.B would like to acknowledge the financial support provided by the German Research Foundation (Deutsche Forschungsgemeinschaft) through the program DFG-Russia, BR4064/5-1. J.v.d.B is also supported by SFB 1143 of the Deutsche Forschungsgemeinschaft. D.V.E also acknowledges the VW Foundation for partial financial support.

[1] R. B. Laughlin, Phys. Rev. B **23**, 5632 (1981).
[2] D. J. Thouless, M. Kohmoto, M. P. Nightingale, and M. den Nijs, Phys. Rev. Lett. **49**, 405 (1982).
[3] F. D. M. Haldane, Phys. Rev. Lett. **61**, 2015 (1988).
[4] C. L. Kane and E. J. Mele, Phys. Rev. Lett. **95**, 146802 (2005).
[5] B. A. Bernevig, T. L. Hughes, and S.-C. Zhang, Science **314**, 1757 (2006).
[6] C.-Z. Chang, J. Zhang, X. Feng, J. Shen, Z. Zhang, M. G. K. Li, Y. Ou, P. Wei, L.-L. Wang, Z.-Q. Ji, Y. Feng, S. J. X. Chen, J. Jia, X. Dai, Z. Fang, S.-C. Zhang, K. He, Y. W. L. Lu, X.-C. Ma, and Q.-K. Xue, Science **340**, 167 (2013).
[7] M. König, S. Wiedmann, C. Brüne, A. Roth, H. Buhmann, L. W. Molenkamp, X.-L. Qi, and S.-C. Zhang, Science **318**, 766 (2007).
[8] A. Altland and M. R. Zirnbauer, Phys. Rev. B **55**, 1142 (1997).
[9] A. P. Schnyder, S. Ryu, A. Furusaki, and A. W. W. Ludwig, Phys. Rev. B **78**, 195125 (2008).
[10] S. Raghu, X.-L. Qi, C. Honerkamp, and S.-C. Zhang, Phys. Rev. Lett. **100**, 156401 (2008).
[11] N. A. García-Martínez, A. G. Grushin, T. Neupert, B. Valenzuela, and E. V. Castro, Phys. Rev. B **88**, 245123 (2013).
[12] M. Daghofer and M. Hohenadler, Phys. Rev. B **89**, 035103 (2014).
[13] J. Motruk, A. G. Grushin, F. de Juan, and F. Pollmann, Phys. Rev. B **92**, 085147 (2015).
[14] S. Capponi and A. M. Läuchli, Phys. Rev. B **92**, 085146 (2015).
[15] K. Sun, H. Yao, E. Fradkin, and S. A. Kivelson, Phys. Rev. Lett. **103**, 046811 (2009).
[16] J. W. F. Venderbos, M. Manzardo, D. V. Efremov, J. van den Brink and C. Ortix, Phys. Rev. B **93**, 045428 (2016).
[17] H.-Q. Wu, Y.-Y. He, C. Fang, Z. Y. Meng, and Z.-Y. Lu, Phys. Rev. Lett. **117**, 066403 (2016).
[18] W. Zhu, S.-S. Gong, T.-S. Zeng, L. Fu, and D. N. Sheng, Phys. Rev. Lett. **117**, 096402 (2016).
[19] J. M. Murray and O. Vafek, Phys. Rev. B **89**, 201110(R) (2014).
[20] O. Vafek, Phys. Rev. B **82**, 205106 (2010).
[21] O. Vafek and K. Yang, Phys. Rev. B **81**, 041401(R) (2010).
[22] P. A. Lee and T. V. Ramakrishnan, Rev. Mod. Phys. **57**, 287 (1985).
[23] F. Evers and A. D. Mirlin, Rev. Mod. Phys. **80**, 1355 (2008).
[24] A. A. Nersesyan, A. M. Tsvelik, and F. Wenger, Nucl. Phys. B **438**, 561 (1995).
[25] H.-H. Hung, A. Barr, E. Prodan, and G. A. Fiete, Phys. Rev. B **94**, 235132 (2016).
[26] D. V. Efremov, M. M. Korshunov, O. V. Dolgov, A. A. Golubov, and P. J. Hirschfeld, Phys. Rev. B **84**, 180512 (2011).
[27] D. V. Efremov, A. A. Golubov, and O. V. Dolgov, New J. Phys. **15**, 013002 (2013).
[28] M. M. Korshunov, D. V. Efremov, A. A. Golubov, and O. V. Dolgov, Phys. Rev. B **90**, 134517 (2014)
[29] B. I. Halperin, Phys. Rev. B **25**, 2185 (1982).
[30] T. Stauber, F. Guinea, and M. A. H. Vozmediano, Phys. Rev. B **71**, 041406(R) (2005).
[31] E. Fradkin, S. A. Kivelson, M. J. Lawler, J. P. Eisenstein, and A. P. Mackenzie, Annu. Rev. Condens. Matter Phys. **1**, 153 (2010).
[32] A. Altland, B. D. Simons, and M. R. Zirnbauer, Phys. Rep. **359**, 283 (2002).
[33] P. A. Lee, N. Nagaosa, and X.-G. Wen, Rev. Mod. Phys. **78**, 17 (2006).
[34] K. S. Novoselov, A. K. Geim, S. V. Morozov, D. Jiang, M. I. Katsnelson, I. V. Grigorieva, S. V. Dubonos, and A. A. Firsov, Nature (London) **438**, 197 (2005).
[35] I. L. Aleiner and K. B. Efetov, Phys. Rev. Lett. **97**, 236801 (2006); M. S. Foster and I. L. Aleiner, Phys. Rev. B **77**, 195413 (2008).
[36] A. H. Castro Neto, F. Guinea, N. M. R. Peres, K. S. Novoselov, and A. K. Geim, Rev. Mod. Phys. **81**, 109 (2009).
[37] S. Das Sarma, S. Adam, E. H. Hwang, and E. Rossi, Rev. Mod. Phys. **83**, 407 (2011).
[38] V. N. Kotov, B. Uchoa, V. M. Pereira, F. Guinea, and A. H. Castro Neto, Rev. Mod. Phys. **84**, 1067 (2012).
[39] A. W. W. Ludwig, M. P. A. Fisher, R. Shankar, and G. Grinstein, Phys. Rev. B **50**, 7526 (1994).
[40] J. E. Furneaux, S. V. Kravchenko, W. E. Mason, G. E. Bowker, and V. M. Pudalov, Phys. Rev. B **51**, 17227 (1995).
[41] J. Ye and S. Sachdev, Phys. Rev. Lett. **80**, 5409 (1998); J. Ye, Phys. Rev. B **60**, 8290 (1999).
[42] M. Z. Hasan and C. L. Kane, Rev. Mod. Phys. **82**, 3045 (2010).

[43] S. Sachdev, *Quantum Phase Transitions* (Cambridge University Press, Cambridge, 1999).
[44] J. Wang, G.-Z. Liu, and H. Kleinert, Phys. Rev. B **83**, 214503 (2011).
[45] K. G. Wilson, Rev. Mod. Phys. **47**, 773 (1975).
[46] J. Polchinski, arXiv:hep-th/9210046.
[47] R. Shankar, Rev. Mod. Phys. **66**, 129 (1994).
[48] V. Cvetkovic, R. E. Throckmorton, and O. Vafek, Phys. Rev. B **86**, 075467 (2012).
[49] K. Sun and E. Fradkin, Phys. Rev. B **78**, 245122 (2008).
[50] Y. D. Chong, X.-G. Wen, and M. Soljaĉić, Phys. Rev. B **77**, 235125 (2008).
[51] See Supplemental Material at http://link.aps.org/supplemental/10.1103/PhysRevB.96.201104 for the effective theory for both checkerboard and bilayer honeycomb lattice, and the corresponding coupled flow equations, fixed points, and susceptibilities for all three sorts of disorders.
[52] O. Vafek, J. M. Murray, and V. Cvetkovic, Phys. Rev. Lett. **112**, 147002 (2014).
[53] Y. Huh and S. Sachdev, Phys. Rev. B **78**, 064512 (2008).
[54] J.-H. She, J. Zaanen, A. R. Bishop, and A. V. Balatsky, Phys. Rev. B **82**, 165128 (2010).
[55] J. Wang and G.-Z. Liu, New J. Phys. **15**, 073039 (2013).
[56] J.-H. She, M. J. Lawler, and E.-A. Kim, Phys. Rev. B **92**, 035112 (2015).
[57] F. Kirtschig, J. van den Brink, and C. Ortix, arXiv:1503.07456.
[58] D. R. Nelson, Phys. Rev. B **11**, 3504 (1975).
[59] E. McCann and V. I. Fal'ko, Phys. Rev. Lett. **96**, 086805 (2006).
[60] J. Nilsson, A. H. Castro Neto, F. Guinea, and N. M. R. Peres, Phys. Rev. B **78**, 045405 (2008).
[61] Y. Lemonik, I. L. Aleiner, C. Toke, and V. I. Fal'ko, Phys. Rev. B **82**, 201408 (2010).
[62] R. Nandkishore and L. Levitov, Phys. Rev. B **82**, 115124 (2010).
[63] L.-J. Zhu, V. Aji, and C. M. Varma, Phys. Rev. B **87**, 035427 (2013).
[64] H. Min, G. Borghi, M. Polini, and A. H. MacDonald, Phys. Rev. B **77**, 041407(R) (2008).
[65] R. Nandkishore and L. Levitov, Phys. Rev. Lett. **104**, 156803 (2010).
[66] C. Y. Hou, C. Chamon, and C. Mudry, Phys. Rev. Lett. **98**, 186809 (2007).
[67] R. E. Throckmorton and O. Vafek, Phys. Rev. B **86**, 115447 (2012).
[68] Y. Lemonik, I. L. Aleiner, and V. I. Fal'ko, Phys. Rev. B **85**, 245451 (2012).
[69] M. M. Scherer, S. Uebelacker, and C. Honerkamp, Phys. Rev. B **85**, 235408 (2012).
[70] M. Kharitonov, Phys. Rev. B **86**, 195435 (2012).